Editors' Suggestion

Fractional AC Josephson effect in a topological insulator proximitized by a self-formed superconductor

Ilan T. Rosen,[1,2] Christie J. Trimble,[3] Molly P. Andersen,[4,2] Evgeny Mikheev,[5,2] Yanbin Li,[4] Yunzhi Liu,[4] Lixuan Tai,[6] Peng Zhang,[6] Kang L. Wang,[6] Yi Cui,[4,2] M. A. Kastner,[5,2,7] James R. Williams,[3,5,2] and David Goldhaber-Gordon[5,2,*]

[1]*Department of Applied Physics, Stanford University, Stanford, California 94305, USA*

[2]*Stanford Institute for Materials and Energy Sciences, SLAC National Accelerator Laboratory, Menlo Park, California 94025, USA*

[3]*Joint Quantum Institute and Quantum Materials Center, Department of Physics, University of Maryland, College Park, Maryland 20742, USA*

[4]*Department of Materials Science and Engineering, Stanford University, Stanford, California 94305, USA*

[5]*Department of Physics, Stanford University, Stanford, California 94305, USA*

[6]*Department of Electrical Engineering, University of California, Los Angeles, California 90095, USA*

[7]*Department of Physics, Massachusetts Institute of Technology, Cambridge, Massachusetts 02139, USA*

(Received 4 October 2021; revised 26 June 2024; accepted 30 July 2024; published 21 August 2024)

A lateral Josephson junction in which the surface of a three-dimensional (3D) topological insulator (TI) serves as the weak link should support topologically protected excitations related to Majorana fermions. The resulting 4π-periodic current-phase relationship could be detected under high-frequency excitation by the suppression of odd Shapiro steps. Here, we demonstrate such devices through the self-formation of a Pd-Te superconducting layer from a telluride TI and observe suppressed first and third Shapiro steps. Other devices, including those where the Pd-Te layer is bolstered by an additional Al layer, show no suppression of Shapiro steps, a difference supported by simulations. Though we rule out the known trivial causes of suppressed Shapiro steps in our devices, we nevertheless argue that corroborating measurements and disorder-aware theoretical descriptions of these systems are needed before confidently claiming the observation of Majorana states.

DOI: 10.1103/PhysRevB.110.064511

I. INTRODUCTION

The surface of a three-dimensional (3D) topological insulator (TI) hosts a nondegenerate band of massless Dirac fermions [1]. Proximity to an *s*-wave superconductor is predicted to mediate $p+ip$ pairing in the topological surface state, a consequence of the spin texture of the Dirac band. A Josephson junction with a TI weak link should support topologically protected gapless Andreev bound states (ABSs) known as Majorana bound states (MBSs) [2]. MBSs impart a 4π-periodic component to the current-phase relationship of the junction, which coexists with the 2π-periodic component from the spectrum of conventional ABSs at higher energies. In principle, 4π periodicity can be detected via the fractional AC Josephson effect: Junction current oscillates at half the normal Josephson frequency for a given voltage, or equivalently DC junction voltage is twice as large for a given frequency of AC current. Thus, under radiofrequency (RF) irradiation, Shapiro steps $V = nhf/2e$ with odd n should be absent.

Claims for the observation of the fractional AC Josephson effect have been made in a variety of topological systems, including nanowires with spin-orbit coupling [3,4], strained 3D HgTe [5], two-dimensional (2D) HgTe [6,7], Dirac semimetals [8], Bi_2Se_3 [9], and $(BiSb)_2Te_3$ [10,11]. Among these works, only in 2D HgTe has suppression of odd Shapiro steps beyond the first been observed [6]. Suppression of the first Shapiro step, however, can result from trivial effects in Josephson junctions, including Joule overheating [9] and underdamping [12]. Therefore, the suppression of higher odd Shapiro steps is a crucial step in eliminating the ambiguity surrounding claims of 4π periodicity. Landau-Zener transitions (LZTs) suppress the expression of the first and higher odd Shapiro steps but only in devices with near-unity interface transparency between superconductor and weak link [13], offering a clear-cut way to rule out this mechanism.

Fabricating high-quality Josephson junctions with TI weak links is technically challenging. A number of groups have demonstrated superconducting contact to exfoliated flakes from single crystals in the Bi_2Se_3 family of TIs [14–21], yet even if Majorana physics were confirmed, the impact of approaches reliant on individually exfoliated flakes would be limited by the need for scalability and reproducibility. Aspiring toward the scientific imperative to compile results from many devices alongside the technological goal of a scalable quantum information architecture based on Majorana modes [22], it is vital to transition to films grown at wafer scale by molecular beam epitaxy (MBE) [23], yet progress in MBE-based platforms has been hampered by poor superconductor/TI (S/TI) interface quality, the difficulty in protecting fragile chalcogenides during device fabrication [24], and unwanted doping of the TI due to charge transfer across the S/TI interface.

In this paper, we fabricate lateral Josephson junctions with TI weak links through the self-formation of a superconducting Pd-Te layer, as pioneered in Ref. [25]. Using a variety

*Contact author: goldhaber-gordon@stanford.edu

of imaging techniques and low-frequency electrical measurements, we show that our fabrication process (1) yields a S/TI interface with moderate transparency, while (2) minimizing damage to the TI film and (3) nearing a work-function match between superconductor and TI. Under RF excitation, we observe suppression of the first and third Shapiro steps in one device, and suppression of the first step in more devices. Other devices express all Shapiro steps. We argue that our observations result from neither LZTs nor junction hysteresis nor bias-dependent resonances [26]. Across devices, simulations in which the 4π-periodic component comprises a few percent of the total junction supercurrent generally match the observed expression of Shapiro steps. Our results therefore constitute compelling evidence in favor of the presence of MBSs in the junctions, yet several differences between measurement and simulations signal that our description of the junction dynamics is incomplete. We highlight the need for corroborating results and for further exploration of disordered S/TI interfaces ahead of definitive conclusions about Majorana states.

II. METHODS

To isolate Majorana physics in TI weak-link junctions, the S/TI heterostructure must achieve sufficient electrical transparency at the S/TI interface while preserving the topological character of the TI. The former condition, well known from superconductor/semiconductor structures [27–31], is required to open a pairing gap in the topological surface states via the proximity effect. The latter condition is specific to topological matter and is particularly difficult due to the susceptibility of the Bi_2Se_3 family of materials to unwanted doping. The Fermi level of a TI should lie within the bulk band gap so that the topological surface states are not shunted by trivial bulk states. In MBE-grown films, the Fermi level is commonly tuned by adjusting the composition of ternary $(Bi_xSb_{1-x})_2Te_3$ (BST) and quarternary $(Bi_xSb_{1-x})_2(Se_yTe_{1-y})_3$ alloys, compensating for charged disorder including Te vacancies, Sb-Te antisite defects, and interfacial defects [32–34]. However, postgrowth device fabrication can introduce additional disorder, destroying the delicate charge balance or introducing midgap defect states [24]. Furthermore, charge transfer from the superconductor can substantially dope the TI unless their work functions are closely matched.

Two recent technologies have enabled transparent S/TI interfaces and, in turn, realization of the Josephson effect in MBE-grown TI films. One approach is to grow the TI and superconductor structures entirely *in situ* using stencil lithography to facilitate patterning, an approach leading to the observation of a suppressed first Shapiro step [10]. In this paper, we follow a second approach, the self-formation of a superconducting Pd-Te layer through the laterally patterned *ex situ* deposition of Pd [25]. Though, in general, chemical reactions with deposited metal are problematic [35] (for example, depositing Al on Sb_2Te_3 might create a barrier layer of AlSb, a ∼2 eV band gap semiconductor), here, the reactivity between Pd and Te is desired.

Our devices are based on an 8-quintuple-layer-thick $(Bi_{0.4}Sb_{0.6})_2Te_3$ film grown by MBE on a GaAs substrate. We pattern resist masks for Josephson junctions using a low-voltage electron beam lithography process developed to impart minimal beam damage to the TI film [24,36]. Lateral Josephson junctions are fabricated by depositing 11 nm Pd on a resist-masked BST film in an electron beam evaporator, forming a superconducting Pd-Te alloy (with residual Bi and Sb) in exposed regions, while the BST weak link is masked [Fig. 1(a)]. After depositing the Pd and then liftoff, unwanted areas of BST are etched by Ar ion milling. In some devices, the etched region abuts the Josephson junction weak link, terminating the transverse extent of bound states, whereas in other devices, a region of BST film surrounding the weak link remains unetched; we noticed no corresponding difference in electronic transport. Our methodology and the junction geometries are described further in the Supplemental Material [36].

Junctions have geometric length of roughly $L = 160$ nm (parallel to current flow; measured by scanning electron microscopy) and width $W = 2\,\mu$m (transverse to current flow). Throughout this paper, critical temperatures, fields, and currents are defined by the condition $R = R_N/2$, where R_N is the normal state resistance. The critical temperature and field of the superconductor are determined by transport through a strip of the superconductor with no weak link. Both devices presented here were fabricated simultaneously on the same chip. Three more devices on the same chip and several devices fabricated separately on other chips from the same BST film growth are discussed in the Supplemental Material [36]. Separate dilution refrigerators were used for low-frequency characterization measurements of Device 1 (at Stanford University; base temperature 30 mK) and Shapiro step measurements of Device 2 (at University of Maryland; base temperature 50 mK). All measurements used standard lock-in techniques; for Shapiro step measurements, microwave excitations were combined with low-frequency excitations at source electrodes.

A. Characterization

Here, we summarize findings from material and device characterization measurements, which are presented in greater detail in the Supplemental Material [36].

1. Topological insulator

The electronic characteristics of the BST film are determined by Hall geometry measurements at 30 mK. The sheet resistivity of the film $\rho_{xx} = 1.55\,\text{k}\Omega$, from n-type charge carriers with density $n = 4.8 \times 10^{12}$ cm^{-2}, mobility $\mu = 820$ cm^2/Vs, and elastic mean free path $\ell_e = \hbar k_F \mu/e = 15$ nm. The film has negative magnetoconductance, indicating weak antilocalization [37,38]. Fitting the magnetoconductance by the Hikami-Larkin-Nagaoka formula yields a phase coherence length $\ell_\phi = 850$ nm [39], which provides an estimate for the inelastic mean free path ℓ_i.

2. Junction characteristics

A cross-sectional image of a portion of a junction, taken in a transmission electron microscope, is shown in Fig. 1(b). The deposited Pd diffuses vertically through the entire BST film and into the GaAs substrate. Excess Pd forms grains on top of

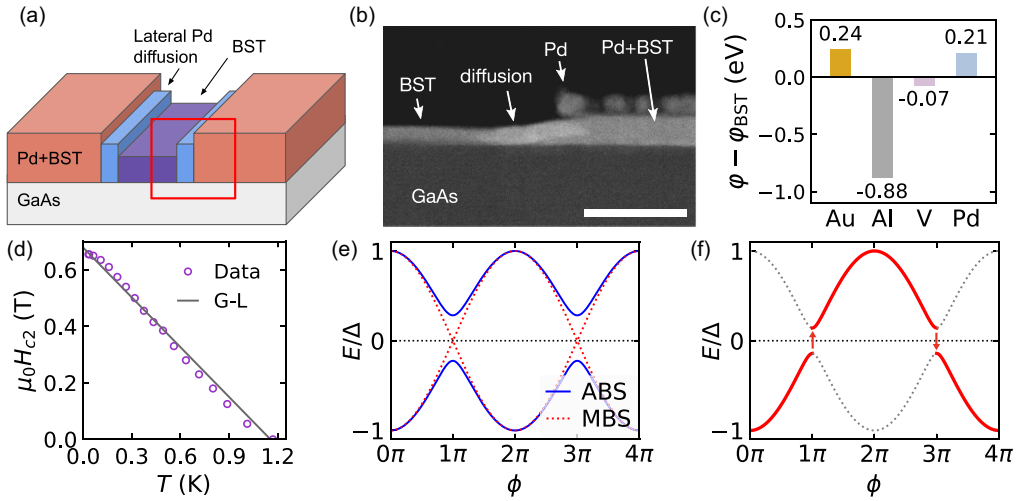

FIG. 1. Junctions with a self-formed Pd-Te superconductor. (a) Schematic of a junction (not to scale). The superconductor/topological insulator (S/TI) interface is lateral, unlike most S/normal metal interfaces, where the superconductor sits on top of the normal metal. At the interface is a region where Pd diffuses laterally into the weak link. (b) Cross-sectional high-angle annular dark-field (HAADF) image of a portion of a junction indicated by the red box in (a). At left, the BST weak link. At right, the superconducting Pd-Te region, with greater film thickness due to Pd incorporated into the BST. Excess Pd has formed grains atop the film. At center, Pd has diffused laterally into the weak link by ∼40 nm. Scale bar, 50 nm. (c) The work function φ of various contact metals referenced to the work function of the BST film φ_{BST}, measured by Kelvin probe force microscopy. (d) Out-of-plane critical field vs temperature of the Pd-Te superconductor (purple circles), and a fit (gray line) to Ginzburg-Landau (G-L) theory for out-of-plane field. (e) Theoretical spectrum of an Andreev bound state (ABS; blue line; 2π periodicity) and a Majorana bound state (MBS; red dashed line; 4π-periodicity). (f) An excitation (red line) traversing a 2π-periodic ABS (gray dashed line) as the phase ϕ across the junction evolves, with Landau-Zener transitions (LZTs; red arrows) at $\phi = \pi$ and 3π, imparting a 4π-periodic component to the current-phase relationship.

the film. Pd diffuses laterally into the weak link by ∼40 nm. These findings are corroborated by energy-dispersive x-ray spectroscopy, x-ray photoelectron spectroscopy, and scanning Auger electron spectroscopy.

Since Pd diffuses through the full vertical extent of the film, regions where Pd has been deposited have no remaining TI layer. The direction of current flow at the edge of the weak link is therefore normal to the S/TI interface, as sketched in Fig. 1(a). This geometry differs from that of junctions based on deposited elemental superconductors, which sit atop the TI so that current flows parallel to the interface plane.

3. *Work function offsets*

Many superconductors have work functions substantially offset from that of members of the Bi_2Se_3 family. For example, the work functions of bulk Al and Nb are less than that of Bi_2Te_3 by nearly 1 eV [40,41], which exceeds the 0.3 eV bulk band gap of Bi_2Te_3. At a transparent interface between these two materials, charge transfer should dope the TI, moving the chemical potential into the bulk conduction band and admitting topologically trivial Cooper pairing. Kelvin probe force microscopy (KPFM) confirms the work function of evaporated Al is offset from that of BST by −880 meV [Fig. 1(c)].

The work functions of Pd and Pd-Te alloys are substantially closer. KPFM indicates a work function offset of ∼200 meV between Pd-Te and BST [Fig. 1(c)].

4. *Electrical properties*

The Pd-Te superconductor has critical temperature $T_c = 1.17$ K, normal state sheet resistance 100 Ω, and critical field $\mu_0 H_{c2} = 655$ mT [Fig. 1(d)], which implies a coherence length $\xi = 22.4$ nm through the Ginzburg-Landau relation $\xi^2 = \frac{\Phi_0}{2\pi H_{c2}}$. The devices therefore fall in the long dirty junction limit $\xi, \ell_e \ll L$.

The current-voltage relationship of Device 1 is shown in Fig. 2(a). Supercurrent flows across the junction below the critical current $I_c = 370$ nA. Between the critical current and ∼500 nA are a series of sudden increases in the voltage, which are discussed in the Supplemental Material [36]. At higher currents, the differential resistance returns to the normal state resistance $R_N = 146\,\Omega$. Extrapolating the normal section of the current-voltage relationship to zero voltage yields an excess current $I_e = 136$ nA. The critical and excess currents are shown as a function of temperature in Fig. 2(b). Although Pd-Te superconductivity may not be well described by Bardeen-Cooper-Schrieffer (BCS) theory, if we take the superconducting gap as $\Delta_{BCS} = 1.76 k_B T_c$ we arrive at the dimensionless figures of merit $eI_c R_N/\Delta_{BCS} = 0.30$ and $eI_e R_N/\Delta_{BCS} = 0.10$. Naively, the latter implies a junction transparency $\tau \approx 0.25$ according to BTK theory [42]. Device 2 has $eI_e R_N/\Delta_{BCS} = 0.29$, implying $\tau \approx 0.3$. We present a nuanced analysis of the junction transparency in the Supplemental Material [36]. The current-voltage relationship is not hysteretic, indicating that the junction is overdamped (consistent with our estimation of the Stewart-McCumber parameter $\beta_C \sim 10^{-4}$) and that Joule overheating is not limiting the retrapping current [43].

Figure 3 shows the resistance of Device 1 in a perpendicular magnetic field. The critical current displays the typical Fraunhofer pattern, approaching zero at nonzero integer multiples of a characteristic magnetic field $B_0 = \Phi_0/L_{\text{eff}}W$, where

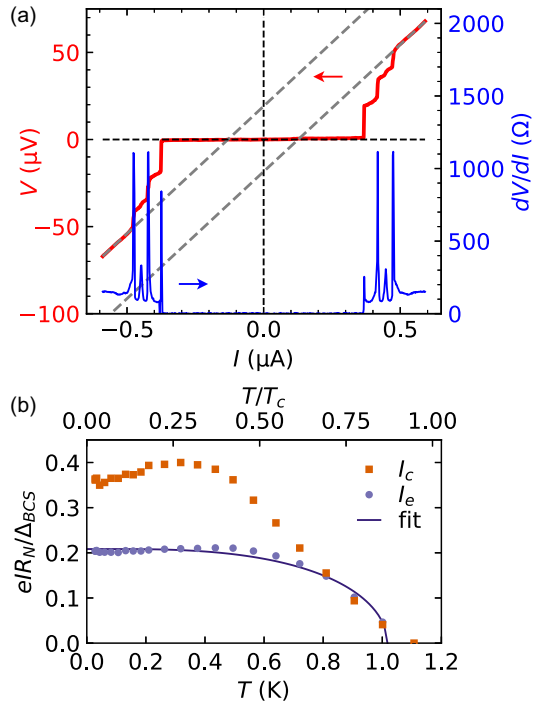

FIG. 2. Junctions with Pd-Te superconducting leads under DC bias. (a) Voltage and differential resistance of Device 1 as a function of current bias. (Dashed lines) Linear fits at high bias. The excess current is determined by the intercept of these lines with $V = 0$. (b) Critical current and excess current of Device 2 as a function of temperature. (Dashed line) The temperature dependence of the Bardeen-Cooper-Schrieffer (BCS) superconducting gap fit to the excess current [36].

L_{eff} is the effective junction length. A fit yields $L_{\text{eff}} = 1.1\,\mu\text{m}$, which is significantly larger than the geometric length of the junction $L \approx 160$ nm. We find this disparity surprising, as we expect minimal flux focusing by the thin Pd-Te leads.

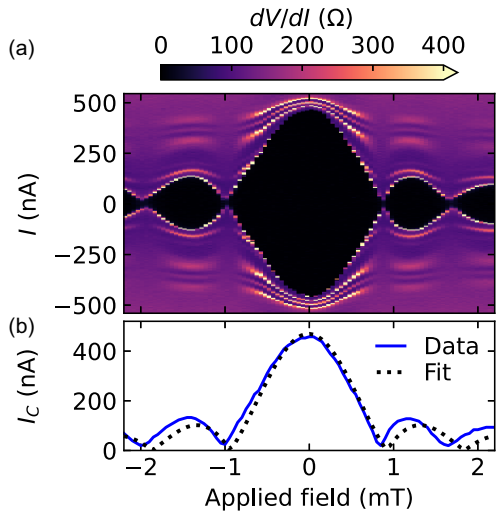

FIG. 3. Device 1 in a perpendicular magnetic field. (a) Differential resistance at finite bias. (b) The extracted critical current. (Dashed line) Fit to the Fraunhofer pattern.

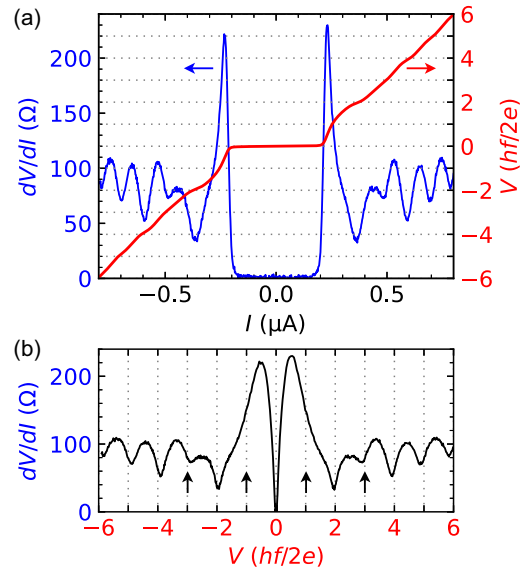

FIG. 4. Current-voltage relationship in Device 2 under 4.3 GHz excitation (nominal power −33.5 dBm). (a) (Left) Differential resistance vs current bias, and (right) DC voltage, obtained by numerical integration of the differential resistance. (b) The same data shown parametrically, emphasizing the suppression of the first and third Shapiro steps, as indicated by the arrows.

B. Junctions under RF irradiation

The low-frequency differential resistance of Device 2 when subjected to an additional RF drive at frequency $f = 4.3$ GHz is shown in Fig. 4. Outside of the central zero-resistance region at low bias and low RF power are a series of regions of low differential resistance at finite DC voltage. These regions are centered at voltages $nhf/2e$ for integer n, expressing the nth Shapiro steps. The strengths of differential resistance dips associated with the first and third Shapiro steps are suppressed relative to those of the second and fourth steps.

The evolution of the differential resistance with RF excitation power is shown at different RFs in Figs. 5(a)–5(c). The development of Shapiro steps is clarified by the histograms in Figs. 5(d)–5(f) formed by grouping the data points (equally spaced in DC current) into DC voltage bins, so that Shapiro steps are visible as bright streaks. At 4.3 GHz, the weights of the first and third Shapiro steps are suppressed at low powers in comparison with those of the second and fourth steps and develop only at higher powers. The third step is recovered as the RF is increased to 5.7 GHz, as is the first step at 10 GHz. Figures 5(g)–5(i) present another visualization of the formation of Shapiro steps by showing the differential resistance at the voltages corresponding to the first four Shapiro steps as a function of RF power. At 4.3 GHz, even steps form at lower RF power than odd steps, as indicated by the lower differential resistance, whereas at 10 GHz, the steps form sequentially. We present additional visualizations of these data in Sec. S8 of the Supplemental Material [36], along with data from three further devices, in two of which we observe suppression of the first Shapiro step.

The suppression of odd Shapiro steps is an expected signature of the presence of a MBS. The ABS spectrum of a conventional Josephson junction is 2π-periodic, leading to a

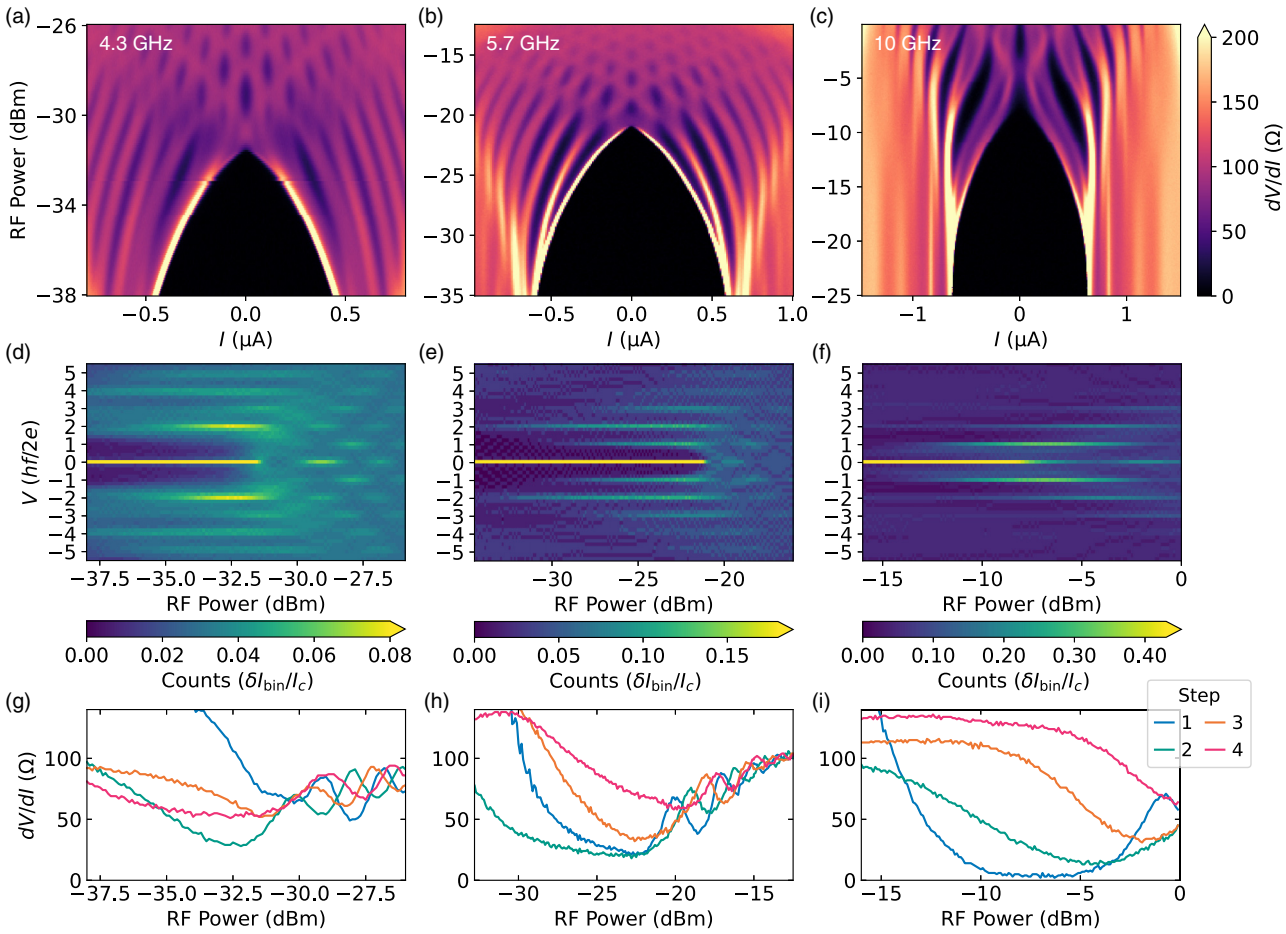

FIG. 5. Shapiro steps in Device 2. (a)–(c) Differential resistance as a function of bias current and radiofrequency (RF) excitation power. (d)–(f) Corresponding histograms of measured data points within DC voltage bins, shown in normalized units $hf/2e$, with the number of counts in each bin normalized as a fraction of the critical current. The nth Shapiro step appears at voltage $nhf/2e$. (g)–(i) The value of the differential resistance at the voltage corresponding first through fourth Shapiro step, as a function of RF power. The frequency of RF excitation is (a), (d), and (g) $f = 4.3$ GHz, (b), (e), and (h) 5.7 GHz, and (c), (f), and (i) 10 GHz.

2π-periodic current phase relationship and Shapiro steps at voltages $V = nhf/2e$ for integer n. The 2π-periodicity results from an avoided crossing of the two branches of the lowest-energy ABS at $\phi = \pi$ [Fig. 1(e)], a consequence of scattering in the junction or at interfaces. However, contact to a superconductor is expected to induce effective p-wave pairing in a TI [2], and a junction between p-wave superconductors should support a pair of MBSs [44–46]. At $\phi = \pi$ and 3π, the two MBSs do not couple and are therefore bound to zero energy. Because these states differ in fermion parity (unlike ABS, which tunnel charge $2e$), this picture should be valid provided the Majorana modes are spatially separated and there are no quasiparticle excitations [47], requiring $k_B T \ll \Delta_{\mathrm{BCS}}$.

The current-phase relationship of the junction therefore gains a 4π-periodic component, which coexists with the 2π-periodic term [48]. At high RF power and frequency, the 2π component is expected to dominate the junction dynamics, but at low RF power and frequency, the 4π component may dominate, leading to a suppression of Shapiro steps with odd n [9].

The observation of suppressed odd Shapiro steps does not necessarily imply the presence of a Majorana mode, yet the known alternative mechanisms do not apply to our devices. First, the lowest Shapiro steps can be suppressed at low RF power in underdamped junctions [12] as well as in overdamped junctions with substantial self-heating [49,50]. The small capacitance and lack of hysteresis in our junctions is not consistent with these effects; furthermore, these effects cannot suppress the third step while leaving the second step intact.

Second, suppression of the first and third Shapiro steps due to LZTs between upper and lower ABS branches near $\phi = \pi$ [Fig. 1(f)] has been predicted [51,52] and recently observed in a lateral Josephson junction based on a topologically trivial InAs weak link [13], enabled by exceptionally high interface transparency. The probability of a LZT is

$$P = \exp\left[-\frac{\pi(1-\tau)\Delta}{eV}\right], \tag{1}$$

which is significant only when $\tau \approx 1$ [53]. Our junctions have τ of $\sim$0.3, far from the ultrahigh-transparency regime in which LZTs occur.

Third, recent computational work has suggested that the nth Shapiro step can be suppressed by unwanted device resonances if the resonances occur at DC voltages at or near $nhf/2e$ [26]. We do observe resonances above the critical current of our devices. The resonances appear at fixed voltages

with varying field and temperature, even close to T_c, which is inconsistent with multiple Andreev reflection and Fiske resonance (see Sec. S6 in the Supplemental Material [36]). Instead, we suggest that the resonances arise from radiative coupling between the device and cavity modes of the cryostat or of the electrical wiring. However, regardless of their origin, resonances do not clearly explain the suppression of odd Shapiro steps in our devices, as we observe suppression of the first step throughout the range 2.5 GHz (the lowest frequency at which Shapiro steps clearly develop) to 7 GHz, which is inconsistent with resonances appearing at fixed voltages. Therefore, we exclude hysteresis, LZTs, and resonances as alternatives to the presence of MBS to explain the observation of suppressed Shapiro steps.

In Sec. S9 in the Supplemental Material [36], we present numerical simulations of the resistance of the device under microwave irradiation based on the resistively shunted junction (RSJ) model:

$$\frac{V}{R_N} + I_{2\pi}\sin(\phi) + I_{4\pi}\sin\left(\frac{\phi}{2}\right) = I_{\mathrm{DC}} + I_{\mathrm{RF}}\sin(ft), \quad (2)$$

where $V = \hbar\dot{\phi}/2e$ is the voltage across the junction, ϕ is the phase across the junction, R_N is the normal-state resistance, $I_{2\pi\,(4\pi)}$ is the 2π (4π)-periodic portion of the critical current, f is the microwave irradiation frequency, and $I_{\mathrm{DC\,(RF)}}$ are the DC and microwave-frequency current biases, respectively [26,54]. Values for R_N and the total critical current $I_C = I_{2\pi} + I_{4\pi}$ are taken from junction characterization measurements. Simulations of Device 2 feature noticeable suppression of odd Shapiro steps when $I_{4\pi}$ is just a few percent of I_C, confirming the plausibility of interpreting suppressed Shapiro steps as a signature of MBS. Experimental and simulated results differ in the widths of the regions between adjacent steps. The differences are discussed in Sec. S9 in the Supplemental Material [36] and may indicate that the current-phase relationship in Eq. (2) is an incomplete model of the junction dynamics.

C. Junctions with Al

A drawback of our methodology is the short coherence length of the Pd-Te superconductor, which places our devices near the long junction regime [36]. We attempt to bolster the superconducting coherence length of the junction leads by evaporating 65 nm Al immediately after depositing 5 nm Pd on the BST film. The hybrid Al/Pd-Te superconductor has critical temperature 780 mK (whereas evaporated Al alone has T_c of roughly 1.3 K), and critical field 13 mT. Compared with junctions with Pd-Te alone, junctions with hybrid superconducting leads have similar low-frequency transport characteristics, but lower critical currents and excess currents (in some devices, $I_e < 0$) [36].

Since the coherence length is increased in devices with the hybrid superconductor, but the junction length is unchanged, the junctions should support fewer trivial ABS [55] coexisting with the single MBS. We would therefore expect a proportionally larger 4π-periodic component, leading to more prominent suppression of odd Shapiro steps. Instead, we observe expression of all Shapiro steps in all measured devices (data are shown in Sec. S8 of the Supplemental Material [36]).

In simulations of the devices with Al, presented in Sec. S9 in the Supplemental Material [36], the 4π-periodic bound states must constitute a higher portion of the total critical current—tens of percent—for the suppression of odd Shapiro steps to be visible as compared with the devices with Pd-Te alone. This difference is due to the lower $I_C R_N$ product for devices with Al [36,52]. The simulations therefore indicate that MBSs could possibly be present in all devices, yet are revealed by Shapiro measurements only in devices with the highest transparencies.

In some devices, Shapiro steps are also expressed at fractional multiples of $hf/2e$ [36]. Shapiro steps at multiples of $hf/4e$ have been observed in junctions with exceptionally high transparency [56], reflecting the skewed current-phase relationship in this regime [57], yet our devices have substantially lower transparency. Further work is needed to understand the origin of the fractional steps in our devices.

III. CONCLUSIONS

In this paper, we fabricate Josephson junctions with TI weak links using a self-formed superconductor to provide good interface transparency while minimizing damage to the TI. We observe suppression of the first and third Shapiro steps under low power and low-frequency RF excitation, a hallmark of the fractional AC Josephson effect consistent with the existence of MBSs: topologically protected gapless ABSs. Our data are inconsistent with known topologically trivial sources for the suppression of Shapiro steps and present strong evidence of 4π periodicity in a 3D TI-based Josephson structure.

However, difficulty of obtaining results that are reproducible between devices and that precisely match simulation raises questions for such an interpretation. More work is needed to understand how the structure of the S/TI interface influences Andreev spectra and to confirm that observations of suppressed Shapiro steps reflect 4π periodicity rather than its mere mimicry. Provision of full datasets without postselection, as we have done here, is needed for the community to reach reliable conclusions regarding the existence of Majorana modes.

Measurements of the fractional AC Josephson effect, such as those presented here, can be complemented by corroborative probes of the presence of Majorana modes. MBSs should exist in the core of artificial vortices in proximitized TIs, namely, regions of TI surrounded by a superconductor wound by a phase 2π. An artificial vortex may be realized as a flux-biased superconducting ring or as a phase-biased superconducting trijunction [2]. In both geometries, the presence of a MBS could be corroborated by a zero-bias peak in the conductance spectroscopy of a tunnel probe, analogous to the features sought in semiconducting nanowires [58] and vortex cores of candidate intrinsic p-wave superconductors [59,60]. However, the necessary tunnel contacts to Bi_2Se_3-class TIs are difficult to fabricate *ex situ*. In the Supplemental Material [36], we propose a device based on self-formed superconducting contacts that could address this challenge.

Finally, the Pd-BST heterostructure developed in this paper could be extended to realize a transparent superconducting contact to the quantum anomalous Hall system. Here, the BST

would be replaced with its ferromagnetic analog, the quantum anomalous Hall insulator Cr-$(BiSb)_2Te_3$, and the Pd-Te superconductor would be bolstered by deposition of a large-gap superconductor like Nb immediately following deposition of the Pd (likely needed to overcome depairing due to magnetic exchange).

Note added. While preparing this paper, we became aware of a work with similar methodology [61].

The full dataset is provisioned along with analysis code online [73].

ACKNOWLEDGMENTS

I.T.R., M.P.A., E.M., and Y.Li were supported by the U.S. Department of Energy, Office of Science, Basic Energy Sciences, Materials Sciences and Engineering Division, under Contract No. DE-AC02-76SF00515. I.T.R. additionally acknowledges support from the ARCS foundation. P.Z., L.T., and K.L.W. were supported by the U.S. Army Research Office MURI program under Grant No. W911NF-16-1-0472. AC Josephson measurements of the devices were sponsored by the Army Research Office Award No. W911NF-18-2-0075. Infrastructure and cryostat support were funded in part by the Gordon and Betty Moore Foundation through Grant No. GBMF3429. Part of this work was performed at the nano@Stanford labs, which are supported by the National Science Foundation as part of the National Nanotechnology Coordinated Infrastructure under Award ECCS-1542152.

L.T., P.Z., and K.L.W. developed and grew the BST film. I.T.R. and M.P.A. fabricated and characterized the devices and conducted low-frequency measurements. C.J.T. and J.R.W. measured the devices under RF irradiation. Y.Li, Y.Liu, and Y.C. conducted TEM measurements. I.T.R., C.J.T., M.P.A., E.M., M.A.K., J.R.W., and D.G.-G. analyzed the data. I.T.R. wrote the paper with contributions from all authors.

[1] L. Fu, C. L. Kane, and E. J. Mele, Topological insulators in three dimensions, Phys. Rev. Lett. **98**, 106803 (2007).

[2] L. Fu and C. L. Kane, Superconducting proximity effect and Majorana fermions at the surface of a topological insulator, Phys. Rev. Lett. **100**, 096407 (2008).

[3] L. P. Rokhinson, X. Liu, and J. K. Furdyna, The fractional ac Josephson effect in a semiconductor-superconductor nanowire as a signature of Majorana particles, Nat. Phys. **8**, 795 (2012).

[4] D. Laroche, D. Bouman, D. J. van Woerkom, A. Proutski, C. Murthy, D. I. Pikulin, C. Nayak, R. J. van Gulik, J. Nygård, P. Krogstrup *et al.*, Observation of the 4π-periodic Josephson effect in indium arsenide nanowires, Nat. Commun. **10**, 245 (2019).

[5] J. Wiedenmann, E. Bocquillon, R. S. Deacon, S. Hartinger, O. Herrmann, T. M. Klapwijk, L. Maier, C. Ames, C. Brüne, C. Gould *et al.*, 4 π-periodic Josephson supercurrent in HgTe-based topological Josephson junctions, Nat. Commun. **7**, 10303 (2016).

[6] E. Bocquillon, R. S. Deacon, J. Wiedenmann, P. Leubner, T. M. Klapwijk, C. Brüne, K. Ishibashi, H. Buhmann, and L. W. Molenkamp, Gapless Andreev bound states in the quantum spin Hall insulator HgTe, Nat. Nanotechnol. **12**, 137 (2017).

[7] R. S. Deacon, J. Wiedenmann, E. Bocquillon, F. Domínguez, T. M. Klapwijk, P. Leubner, C. Brüne, E. M. Hankiewicz, S. Tarucha, K. Ishibashi *et al.*, Josephson radiation from gapless Andreev bound states in HgTe-based topological junctions, Phys. Rev. X **7**, 021011 (2017).

[8] C. Li, J. C. de Boer, B. de Ronde, S. V. Ramankutty, E. van Heumen, Y. Huang, A. de Visser, A. A. Golubov, M. S. Golden, and A. Brinkman, 4π-periodic Andreev bound states in a Dirac semimetal, Nat. Mater. **17**, 875 (2018).

[9] K. Le Calvez, L. Veyrat, F. Gay, P. Plaindoux, C. B. Winkelmann, H. Courtois, and B. Sacépé, Joule overheating poisons the fractional ac Josephson effect in topological Josephson junctions, Commun. Phys. **2**, 4 (2019).

[10] P. Schüffelgen, D. Rosenbach, C. Li, T. W. Schmitt, M. Schleenvoigt, A. R. Jalil, S. Schmitt, J. Kölzer, M. Wang, B. Bennemann *et al.*, Selective area growth and stencil lithography for *in situ* fabricated quantum devices, Nat. Nanotechnol. **14**, 825 (2019).

[11] D. Rosenbach, T. W. Schmitt, P. Schüffelgen, M. P. Stehno, C. Li, M. Schleenvoigt, A. R. Jalil, G. Mussler, E. Neumann, S. Trellenkamp *et al.*, Reappearance of first Shapiro step in narrow topological Josephson junctions, Sci. Adv. **7**, eabf1854 (2021).

[12] J. Park, Y.-B. Choi, G.-H. Lee, and H.-J. Lee, Characterization of Shapiro steps in the presence of a 4π-periodic Josephson current, Phys. Rev. B **103**, 235428 (2021).

[13] M. C. Dartiailh, J. J. Cuozzo, B. H. Elfeky, W. Mayer, J. Yuan, K. S. Wickramasinghe, E. Rossi, and J. Shabani, Missing Shapiro steps in topologically trivial Josephson junction on InAs quantum well, Nat. Commun. **12**, 78 (2021).

[14] B. Sacépé, J. B. Oostinga, J. Li, A. Ubaldini, N. J. G. Couto, E. Giannini, and A. F. Morpurgo, Gate-tuned normal and superconducting transport at the surface of a topological insulator, Nat. Commun. **2**, 575 (2011).

[15] J. R. Williams, A. J. Bestwick, P. Gallagher, S. S. Hong, Y. Cui, A. S. Bleich, J. G. Analytis, I. R. Fisher, and D. Goldhaber-Gordon, Unconventional Josephson effect in hybrid superconductor-topological insulator devices, Phys. Rev. Lett. **109**, 056803 (2012).

[16] M. Veldhorst, M. Snelder, M. Hoek, T. Gang, V. K. Guduru, X. L. Wang, U. Zeitler, W. G. van der Wiel, A. A. Golubov, H. Hilgenkamp *et al.*, Josephson supercurrent through a topological insulator surface state, Nat. Mater. **11**, 417 (2012).

[17] C. Kurter, A. D. K. Finck, Y. S. Hor, and D. J. Van Harlingen, Evidence for an anomalous current-phase relation in topological insulator Josephson junctions, Nat. Commun. **6**, 7130 (2015).

[18] M. P. Stehno, V. Orlyanchik, C. D. Nugroho, P. Ghaemi, M. Brahlek, N. Koirala, S. Oh, and D. J. Van Harlingen, Signature of a topological phase transition in the Josephson supercurrent through a topological insulator, Phys. Rev. B **93**, 035307 (2016).

[19] S. Ghatak, O. Breunig, F. Yang, Z. Wang, A. A. Taskin, and Y. Ando, Anomalous Fraunhofer patterns in gated Josephson junctions based on the bulk-insulating topological insulator $BiSbTeSe_2$, Nano Lett. **18**, 5124 (2018).

[20] A. Q. Chen, M. J. Park, S. T. Gill, Y. Xiao, D. Reig-i Plessis, G. J. MacDougall, M. J. Gilbert, and N. Mason, Finite momentum Cooper pairing in three-dimensional topological insulator Josephson junctions, Nat. Commun. **9**, 3478 (2018).

[21] M. Kayyalha, A. Kazakov, I. Miotkowski, S. Khlebnikov, L. P. Rokhinson, and Y. P. Chen, Highly skewed current-phase relation in superconductor–topological insulator–superconductor Josephson junctions, npj Quantum Mater. **5**, 7 (2020).

[22] J. Alicea, Y. Oreg, G. Refael, F. Von Oppen, and M. P. Fisher, Non-Abelian statistics and topological quantum information processing in 1D wire networks, Nat. Phys. **7**, 412 (2011).

[23] J. Shabani, M. Kjaergaard, H. J. Suominen, Y. Kim, F. Nichele, K. Pakrouski, T. Stankevic, R. M. Lutchyn, P. Krogstrup, R. Feidenhans'l *et al.*, Two-dimensional epitaxial superconductor-semiconductor heterostructures: A platform for topological superconducting networks, Phys. Rev. B **93**, 155402 (2016).

[24] M. P. Andersen, L. K. Rodenbach, I. T. Rosen, S. C. Lin, L. Pan, P. Zhang, L. Tai, K. L. Wang, M. A. Kastner, and D. Goldhaber-Gordon, Low-damage electron beam lithography for nanostructures on Bi_2Te_3-class topological insulator thin films, J. Appl. Phys. **133**, 244301 (2023).

[25] M. Bai, F. Yang, M. Luysberg, J. Feng, A. Bliesener, G. Lippertz, A. A. Taskin, J. Mayer, and Y. Ando, Novel self-epitaxy for inducing superconductivity in the topological insulator $(Bi_{1-x}Sb_x)_2Te_3$, Phys. Rev. Mater. **4**, 094801 (2020).

[26] S. R. Mudi and S. M. Frolov, Model for missing Shapiro steps due to bias-dependent resistance, arXiv:2106.00495.

[27] H. Takayanagi, T. Akazaki, and J. Nitta, Observation of maximum supercurrent quantization in a superconducting quantum point contact, Phys. Rev. Lett. **75**, 3533 (1995).

[28] J. Xiang, A. Vidan, M. Tinkham, R. M. Westervelt, and C. M. Lieber, Ge/Si nanowire mesoscopic Josephson junctions, Nat. Nanotechnol. **1**, 208 (2006).

[29] S. Abay, D. Persson, H. Nilsson, H. Xu, M. Fogelström, V. Shumeiko, and P. Delsing, Quantized conductance and its correlation to the supercurrent in a nanowire connected to superconductors, Nano Lett. **13**, 3614 (2013).

[30] P. Krogstrup, N. Ziino, W. Chang, S. Albrecht, M. Madsen, E. Johnson, J. Nygård, C. M. Marcus, and T. Jespersen, Epitaxy of semiconductor-superconductor nanowires, Nat. Mater. **14**, 400 (2015).

[31] M. Kjaergaard, H. J. Suominen, M. P. Nowak, A. R. Akhmerov, J. Shabani, C. J. Palmstrøm, F. Nichele, and C. M. Marcus, Transparent semiconductor-superconductor interface and induced gap in an epitaxial heterostructure Josephson junction, Phys. Rev. Appl. **7**, 034029 (2017).

[32] J. Zhang, C.-Z. Chang, Z. Zhang, J. Wen, X. Feng, K. Li, M. Liu, K. He, L. Wang, X. Chen *et al.*, Band structure engineering in $(Bi_{1-x}Sb_x)_2Te_3$ ternary topological insulators, Nat. Commun. **2**, 574 (2011).

[33] N. Koirala, M. Brahlek, M. Salehi, L. Wu, J. Dai, J. Waugh, T. Nummy, M.-G. Han, J. Moon, Y. Zhu *et al.*, Record surface state mobility and quantum Hall effect in topological insulator thin films via interface engineering, Nano Lett. **15**, 8245 (2015).

[34] M. Salehi, H. Shapourian, I. T. Rosen, M.-G. Han, J. Moon, P. Shibayev, D. Jain, D. Goldhaber-Gordon, and S. Oh, Quantum-Hall to insulator transition in ultra-low-carrier-density topological insulator films and a hidden phase of the zeroth Landau level, Adv. Mater. **31**, 1901091 (2019).

[35] P. Schüffelgen, D. Rosenbach, E. Neumann, M. P. Stehno, M. Lanius, J. Zhao, M. Wang, B. Sheehan, M. Schmidt, B. Gao *et al.*, Stencil lithography of superconducting contacts on MBE-grown topological insulator thin films, J. Cryst. Growth **477**, 183 (2017).

[36] See Supplemental Material at http://link.aps.org/supplemental/10.1103/PhysRevB.110.064511 for detailed methods, additional device characterization, extended data, and simulation results, which also includes Refs. [62–72].

[37] J. Wang, A. M. DaSilva, C.-Z. Chang, K. He, J. K. Jain, N. Samarth, X.-C. Ma, Q.-K. Xue, and M. H. W. Chan, Evidence for electron-electron interaction in topological insulator thin films, Phys. Rev. B **83**, 245438 (2011).

[38] I. T. Rosen, I. Yudhistira, G. Sharma, M. Salehi, M. A. Kastner, S. Oh, S. Adam, and D. Goldhaber-Gordon, Absence of strong localization at low conductivity in the topological surface state of low-disorder Sb_2Te_3, Phys. Rev. B **99**, 201101(R) (2019).

[39] S. Hikami, A. I. Larkin, and Y. Nagaoka, Spin-orbit interaction and magnetoresistance in the two dimensional random system, Prog. Theor. Phys. **63**, 707 (1980).

[40] H. B. Michaelson, The work function of the elements and its periodicity, J. Appl. Phys. **48**, 4729 (1977).

[41] D. Takane, S. Souma, T. Sato, T. Takahashi, K. Segawa, and Y. Ando, Work function of bulk-insulating topological insulator $Bi_{2-x}Sb_xTe_{3-y}Se_y$, Appl. Phys. Lett. **109**, 091601 (2016).

[42] G. E. Blonder, M. Tinkham, and T. M. Klapwijk, Transition from metallic to tunneling regimes in superconducting microconstrictions: Excess current, charge imbalance, and supercurrent conversion, Phys. Rev. B **25**, 4515 (1982).

[43] H. Courtois, M. Meschke, J. T. Peltonen, and J. P. Pekola, Origin of hysteresis in a proximity Josephson junction, Phys. Rev. Lett. **101**, 067002 (2008).

[44] A. Y. Kitaev, Unpaired Majorana fermions in quantum wires, Phys. Usp. **44**, 131 (2001).

[45] L. Fu and C. L. Kane, Josephson current and noise at a superconductor/quantum-spin-Hall-insulator/superconductor junction, Phys. Rev. B **79**, 161408(R) (2009).

[46] R. M. Lutchyn, J. D. Sau, and S. Das Sarma, Majorana fermions and a topological phase transition in semiconductor-superconductor heterostructures, Phys. Rev. Lett. **105**, 077001 (2010).

[47] C. Kane and F. Zhang, The time reversal invariant fractional Josephson effect, Phys. Scr. **T164**, 014011 (2015).

[48] H.-J. Kwon, K. Sengupta, and V. M. Yakovenko, Fractional ac Josephson effect in p- and d-wave superconductors, Eur. Phys. J. B **37**, 349 (2003).

[49] A. De Cecco, K. Le Calvez, B. Sacépé, C. B. Winkelmann, and H. Courtois, Interplay between electron overheating and ac Josephson effect, Phys. Rev. B **93**, 180505(R) (2016).

[50] C. D. Shelly, P. See, I. Rungger, and J. M. Williams, Existence of Shapiro steps in the dissipative regime in superconducting weak links, Phys. Rev. Appl. **13**, 024070 (2020).

[51] P.-M. Billangeon, F. Pierre, H. Bouchiat, and R. Deblock, ac Josephson effect and resonant Cooper pair tunneling emission of a single Cooper pair transistor, Phys. Rev. Lett. **98**, 216802 (2007).

[52] F. Domínguez, F. Hassler, and G. Platero, Dynamical detection of Majorana fermions in current-biased nanowires, Phys. Rev. B **86**, 140503(R) (2012).

[53] D. Averin and A. Bardas, AC Josephson effect in a single quantum channel, Phys. Rev. Lett. **75**, 1831 (1995).

[54] R. A. Snyder, C. J. Trimble, C. C. Rong, P. A. Folkes, P. J. Taylor, and J. R. Williams, Weak-link Josephson junctions made from topological crystalline insulators, Phys. Rev. Lett. **121**, 097701 (2018).

[55] P. F. Bagwell, Suppression of the Josephson current through a narrow, mesoscopic, semiconductor channel by a single impurity, Phys. Rev. B **46**, 12573 (1992).

[56] K. Ueda, S. Matsuo, H. Kamata, Y. Sato, Y. Takeshige, K. Li, L. Samuelson, H. Xu, and S. Tarucha, Evidence of half-integer Shapiro steps originated from nonsinusoidal current phase relation in a short ballistic InAs nanowire Josephson junction, Phys. Rev. Res. **2**, 033435 (2020).

[57] K. K. Likharev, Superconducting weak links, Rev. Mod. Phys. **51**, 101 (1979).

[58] V. Mourik, K. Zuo, S. M. Frolov, S. Plissard, E. P. Bakkers, and L. P. Kouwenhoven, Signatures of Majorana fermions in hybrid superconductor-semiconductor nanowire devices, Science **336**, 1003 (2012).

[59] D. Wang, L. Kong, P. Fan, H. Chen, S. Zhu, W. Liu, L. Cao, Y. Sun, S. Du, J. Schneeloch *et al.*, Evidence for Majorana bound states in an iron-based superconductor, Science **362**, 333 (2018).

[60] Y. Zang, F. Küster, J. Zhang, D. Liu, B. Pal, H. Deniz, P. Sessi, M. J. Gilbert, and S. S. Parkin, Competing energy scales in topological superconducting heterostructures, Nano Lett. **21**, 2758 (2021).

[61] M. Bai, X.-K. Wei, J. Feng, M. Luysberg, A. Bliesener, G. Lippertz, A. Uday, A. A. Taskin, J. Mayer, and Y. Ando, Proximity-induced superconductivity in $(Bi_{1-x}Sb_x)_2Te_3$ topological-insulator nanowires, Commun. Mater. **3**, 20 (2022).

[62] A. H. Castro Neto, F. Guinea, N. M. R. Peres, K. S. Novoselov, and A. K. Geim, The electronic properties of graphene, Rev. Mod. Phys. **81**, 109 (2009).

[63] H. Zhang, C.-x. Liu, X.-l. Qi, X. Dai, Z. Fang, and S.-c. Zhang, Topological insulators in Bi_2Se_3, Bi_2Te_3 and Sb_2Te_3 with a single Dirac cone on the surface, Nat. Phys. **5**, 438 (2009).

[64] P. Dubos, H. Courtois, B. Pannetier, F. K. Wilhelm, A. D. Zaikin, and G. Schön, Josephson critical current in a long mesoscopic S-N-S junction, Phys. Rev. B **63**, 064502 (2001).

[65] C. Ko, Z. Yang, and S. Ramanathan, Work function of vanadium dioxide thin films across the metal-insulator transition and the role of surface nonstoichiometry, ACS Appl. Mater. Interfaces **3**, 3396 (2011).

[66] A. Furusaki, Josephson current carried by Andreev levels in superconducting quantum point contacts, Superlattices Microstruct. **25**, 809 (1999).

[67] B. A. Aminov, A. A. Golubov, and M. Y. Kupriyanov, Quasiparticle current in ballistic constrictions with finite transparencies of interfaces, Phys. Rev. B **53**, 365 (1996).

[68] A. Chrestin, T. Matsuyama, and U. Merkt, Evidence for a proximity-induced energy gap in Nb/InAs/Nb junctions, Phys. Rev. B **55**, 8457 (1997).

[69] M. Octavio, M. Tinkham, G. E. Blonder, and T. M. Klapwijk, Subharmonic energy-gap structure in superconducting constrictions, Phys. Rev. B **27**, 6739 (1983).

[70] M. J. Brahlek, N. Koirala, J. Liu, T. I. Yusufaly, M. Salehi, M.-G. Han, Y. Zhu, D. Vanderbilt, and S. Oh, Tunable inverse topological heterostructure utilizing $(Bi_{1-x}In_x)_2Se_3$ and multichannel weak-antilocalization effect, Phys. Rev. B **93**, 125416 (2016).

[71] G. Jiang, Y. Feng, W. Wu, S. Li, Y. Bai, Y. Li, Q. Zhang, L. Gu, X. Feng, D. Zhang *et al.*, Quantum anomalous Hall multilayers grown by molecular beam epitaxy, Chin. Phys. Lett. **35**, 076802 (2018).

[72] H. Ren, F. Pientka, S. Hart, A. T. Pierce, M. Kosowsky, L. Lunczer, R. Schlereth, B. Scharf, E. M. Hankiewicz, L. W. Molenkamp *et al.*, Topological superconductivity in a phase-controlled Josephson junction, Nature (London) **569**, 93 (2019).

[73] https://zenodo.org/doi/10.5281/zenodo.5893506.